PERGAMON

International Journal of Heat and Mass Transfer 44 (2001) 89–98

International Journal of HEAT and MASS TRANSFER

www.elsevier.com/locate/ijhmt

Heat transfer induced by a body moving in opposition to a flowing fluid

Wu-Shung Fu*, Suh-Jenq Yang

Department of Mechanical Engineering, National Chiao Tung University, 1001 Ta Hsueh Road, Hsinchu 30056, Taiwan

Received 27 May 1999; received in revised form 25 February 2000

Abstract

The heat transfer problem of a body moving in opposition to a flowing fluid in a channel is investigated numerically. This problem belongs to a class of the moving boundary problems and an arbitrary Lagrangian–Eulerian method with a Galerkin finite element method is adopted to analyze this problem. Several different moving velocities of the body and Reynolds numbers are taken into consideration. The results show that the fluid simultaneously replenishes the vacant space induced by the movement of the body and new recirculation zones are formed around the body. These phenomena are quite different from those of the body fixed in the flowing fluid. Heat transfer rates of the body are enhanced remarkably as the body moving in opposition to the flowing fluid. In the computing range, the mean global Nusselt number $\overline{Nu}$ can be estimated by an equation of $0.664(Re\ V_b)^{1/2} - 1.34$.

1. Introduction

The flow and thermal fields induced by the interaction between a flowing fluid and a moving body are very important for application in many engineering problems. From a relative velocity viewpoint, the moving body is traditionally and conveniently regarded as the stationary body in the flowing fluid, in which the relative velocity between the moving body and the fluid is considered. However, the fluid near the body must replenish the vacant space induced by the movement of the body. Strictly speaking, the dynamic problem of the moving body regarded as the stationary body in the flowing fluid is different from that of the body moving in the flowing fluid. Hence, the later situation mentioned above is rarely analyzed by either the Lagrangian or Eulerian description method solely, and can be classified into a kind of the moving boundary problems.

A skillful method named coupled Lagrangian–Eulerian method, which combined the characteristics of the Lagrangian and Eulerian description methods, was proposed by Noh [1] to solve a two-dimensional hydrodynamics problems with moving fluid boundaries. Later, Hirt et al. [2] adopted the concept of the coupled Lagrangian–Eulerian method and renamed it as the arbitrary Lagrangian–Eulerian (ALE) method to solve compressible and incompressible flow fields, and the basic methodology, stability, accuracy, and rezoning of the ALE method were described in detail. Hughes et al. [3], Huerta and Liu [4], and Ramaswamy [5] adopted the ALE method to solve free surface problems of incompressible viscous fluid flow, and the kinematic theory of the ALE method was discussed clearly.

In addition, the ALE method was applied to simulate the fluid–structure interaction [6–11], ma-

* Corresponding author. Tel.: +886-3-5712121; fax: +886-3-5720634.

E-mail address: wsfu@cc.nctu.edu.tw (W.-S. Fu).

0017-9310/01/$ - see front matter
PII: S0017-9310(00)00091-0

Nomenclature

h	dimensional height of the channel, m
H	dimensionless height of the channel ($H = h/\iota$)
d	dimensional distance from the outlet of the channel to the bottom surface of the body, m
D	dimensionless distance from the outlet of the channel to the bottom surface of the body ($D = d/\iota$)
L	dimensionless length of the body ($L = \iota/\iota$)
N_i	shape function
n_e	number of elements
Nu	average global Nusselt number of the body
$\overline{Nu}$	mean global Nusselt number of the body
Nu_X	local Nusselt number on the top or bottom surface of the body
$\overline{Nu_X}$	average local Nusselt number on the top or bottom surface of the body
Nu_Y	local Nusselt number on the lateral surface of the body
$\overline{Nu_Y}$	average local Nusselt number on the lateral surface of the body
p	dimensional pressure, N m^{-2}
p_∞	reference pressure, N m^{-2}
P	dimensionless pressure ($P = (p - p_\infty)/\rho v_0^2$)
Pr	Prandtl number
Re	Reynolds number
t	dimensional time, s
T	dimensional temperature, °C
T_b	dimensional temperature of the body, °C
T_0	dimensional temperature of the inlet fluid, °C
u, v	dimensional velocities in x and y directions, m s^{-1}
U, V	dimensionless velocities in X and Y directions ($U = u/v_0$, $V = v/v_0$)
v_0	dimensional velocity of the inlet fluid, m s^{-1}
v_b	dimensional moving velocity of the body in y-direction, m s^{-1}
V_b	dimensionless moving velocity of the body in Y-direction ($V_b = v_b/v_0$)
$\hat{v}$	dimensional mesh velocity in y-direction, m s^{-1}
$\hat{V}$	dimensionless mesh velocity in Y-direction ($\hat{V} = \hat{v}/v_0$)
w	dimensional width of the channel, m
W	dimensionless width of the channel ($W = w/\iota$)
x, y	dimensional Cartesian coordinates, m
X, Y	dimensionless Cartesian coordinates ($X = x/\iota$, $Y = y/\iota$)

Greek symbols

α	thermal diffusivity, m^2 s^{-1}
ϕ	computational variables
ι	dimensional length of the body, m
λ	penalty parameter
ν	kinematic viscosity, m^2 s^{-1}
θ	dimensionless temperature ($\theta = (T - T_0)/(T_b - T_0)$)
τ	dimensionless time ($\tau = tv_0/\iota$)
$\Delta\tau$	dimensionless time step

Superscripts

(e)	element
m	iteration number
T	transpose matrix

Other

[]	matrix
{}	column vector
⟨⟩	row vector

terial forming process [12–14], and food freeze–drying process [15]. The results obtained by the ALE method were consistent with previous experimental results.

Most of the literature mentioned above investigated the variation of the flow fields only. However, in many industrial applications, such as heat exchangers, electric cooling and fluid machinery, the variations of both the flow and thermal fields induced by the interaction of the fluid and moving body are important; little attention has been focused on this subject.

Consequently, in this paper the ALE method is adopted to investigate numerically the variation of the flow and thermal fields induced by a body moving in opposition to a flowing fluid. For avoiding the distortion and deformation of the computational meshes due to a long movement of the body, an interpolation method is used to reconstruct the distorted and deformed computational meshes. A Galerkin finite element method in conjunction with a backward difference scheme to deal with the time terms is adopted to solve the governing equations. The results show that heat transfer rates are increased and the variations of the flow field are drastic. The mean global Nusselt numbers in the computing range can be estimated by an equation of the form $\overline{Nu} = 0.664(Re\ V_b)^{1/2} - 1.34$.

2. Physical model

The physical model used in this study is sketched in

Fig. 1. There is a vertical channel with height h and width w, respectively. A square body with length ι is set within the channel. FH and EG are the top and bottom surfaces, respectively, FE and HG are the lateral surfaces. The distance from the outlet of the channel to the bottom surface EG of the body is d. The inlet velocity and temperature of the fluid are constant and equal to v_0 and T_0, respectively. The body is maintained at temperature T_b, which is higher than T_0. Initially ($t = 0$), the body is stationary and the fluid is flowing steadily. As the time $t > 0$, the body starts to move upward with a constant velocity v_b, which is opposite to the direction of the flowing fluid. The behavior of the body and fluid are then coupled, and the variation of the flow and thermal fields become time-dependent. As a result, the ALE method is properly utilized to analyze this problem.

In order to facilitate this problem, the following assumptions and the dimensionless variables are made:

1. The fluid is air and the flow field is two-dimensional, incompressible and laminar.
2. The fluid properties are constant and the effect of the gravity is neglected.
3. The no-slip condition is held on the interfaces between the fluid and body.

$$X = \frac{x}{\iota}, \quad Y = \frac{y}{\iota}, \quad U = \frac{u}{v_0}, \quad V = \frac{v}{v_0}, \quad \hat{V} = \frac{\hat{v}}{v_0},$$
$$V_b = \frac{v_b}{v_0}, \quad P = \frac{p - p_\infty}{\rho v_0^2}, \quad \tau = \frac{t v_0}{\iota}, \tag{1}$$
$$\theta = \frac{T - T_0}{T_b - T_0}, \quad Re = \frac{v_0 \iota}{\nu}, \quad Pr = \frac{\nu}{\alpha}.$$

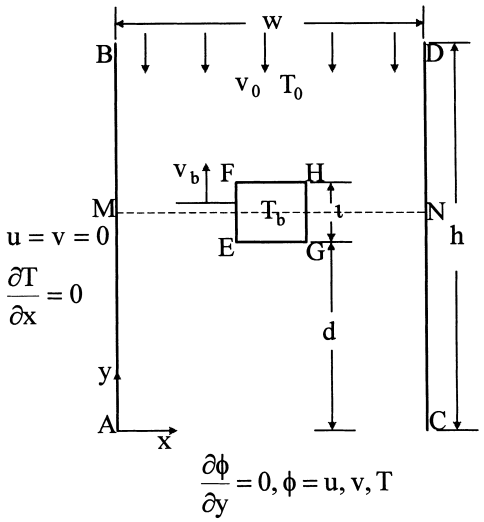

Fig. 1. Physical model.

Based on the above assumptions and dimensionless variables, the dimensionless ALE governing equations [3–5,9,10] are expressed as the following equations:

continuity equation

$$\frac{\partial U}{\partial X} + \frac{\partial V}{\partial Y} = 0, \tag{2}$$

momentum equations

$$\frac{\partial U}{\partial \tau} + U\frac{\partial U}{\partial X} + (V - \hat{V})\frac{\partial U}{\partial Y} = -\frac{\partial P}{\partial X} + \frac{1}{Re}\left(\frac{\partial^2 U}{\partial X^2} + \frac{\partial^2 U}{\partial Y^2}\right), \tag{3}$$

$$\frac{\partial V}{\partial \tau} + U\frac{\partial V}{\partial X} + (V - \hat{V})\frac{\partial V}{\partial Y} = -\frac{\partial P}{\partial Y} + \frac{1}{Re}\left(\frac{\partial^2 V}{\partial X^2} + \frac{\partial^2 V}{\partial Y^2}\right), \tag{4}$$

energy equation

$$\frac{\partial \theta}{\partial \tau} + U\frac{\partial \theta}{\partial X} + (V - \hat{V})\frac{\partial \theta}{\partial Y} = \frac{1}{PrRe}\left(\frac{\partial^2 \theta}{\partial X^2} + \frac{\partial^2 \theta}{\partial Y^2}\right). \tag{5}$$

As the time $\tau > 0$, the boundary conditions are as follows:

on the surfaces AB and CD

$$U = V = 0, \quad \partial\theta/\partial X = 0, \tag{6}$$

on the surface BD (excluding the points B and D)

$$U = 0, \quad V = -1, \quad \theta = 0, \tag{7}$$

on the surface AC (excluding the points A and C)

$$\partial U/\partial Y = \partial V/\partial Y = \partial\theta/\partial Y = 0, \tag{8}$$

on the interfaces EF, FH, EG and GH between the fluid and body

$$U = 0, \quad V = V_b, \quad \theta = 1. \tag{9}$$

3. Numerical method

A Galerkin finite element method and a backward difference scheme, dealing with the time terms, are adopted to solve the governing Eqs. (2)–(5). A penalty function model [16] and Newton–Raphson iteration algorithm are employed to handle the pressure and non-

linear terms in the momentum equations, respectively. The velocity and temperature terms are expressed as quadrilateral and nine-node quadratic isoparametric elements, and the shape function $N_i\,(i=1\text{–}9)$ [17] is utilized as the weighing function. The discretization process of the governing equations is similar to the one used in Ref. [18]. Then, the momentum Eqs. (3) and (4) can be expressed as the following matrix form:

$$\sum_{1}^{n_e}\left([A]^{(e)}+[K]^{(e)}+\lambda[L]^{(e)}\right)\{q\}^{(e)}_{\tau+\Delta\tau}=\sum_{1}^{n_e}\{f\}^{(e)}, \tag{10}$$

where

$$\left(\{q\}^{(e)}_{\tau+\Delta\tau}\right)^T=\langle U_1, U_2, \ldots, U_9, V_1, V_2, \ldots, V_9\rangle^{m+1}_{\tau+\Delta\tau}, \tag{11}$$

$[A]^{(e)}$ includes the mth iteration values of U and V at time $\tau+\Delta\tau$,

$[K]^{(e)}$ includes the shape function, $\hat{V}$ and time differential terms,

$[L]^{(e)}$ includes the penalty function terms,

$\{f\}^{(e)}$ includes the known values of U and V at time τ and mth iteration values of U and V at time $\tau+\Delta\tau$.

The energy equation (5) can be expressed as the following matrix form:

$$\sum_{1}^{n_e}\left([M]^{(e)}+[Z]^{(e)}\right)\{c\}^{(e)}_{\tau+\Delta\tau}=\sum_{1}^{n_e}\{r\}^{(e)}, \tag{12}$$

where

$$\left(\{c\}^{(e)}_{\tau+\Delta\tau}\right)^T=\langle\theta_1, \theta_2, \ldots, \theta_9\rangle_{\tau+\Delta\tau}, \tag{13}$$

$[M]^{(e)}$ includes the values of U and V at time $\tau+\Delta\tau$,

$[Z]^{(e)}$ includes the shape function, $\hat{V}$ and time differential terms,

$\{r\}^{(e)}$ includes the known values of θ at time τ.

In Eqs. (10) and (12), Gaussian quadrature procedure are conveniently used to execute numerical integration. The terms which include the penalty parameter, λ, are integrated by 2×2 Gaussian quadrature, and the other terms are integrated by 3×3 Gaussian quadrature. The value of penalty parameter λ used in this study is 10^6. The frontal method is utilized to solve Eqs. (10) and (12).

For the boundary conditions to be satisfied at the inlet and outlet of the computational domain as shown in Fig. 1, the displacement of the body must be limited so as not to disturb the boundary conditions mentioned above.

As for the mesh velocities, they are linearly distributed and inversely proportional to the distance between the node of the computational meshes and the body. The mesh velocities near the body are faster than those near the boundaries of the computational domain. Moreover, the magnitude of the boundary layer thickness on the body surface is extremely small and can be estimated by $Re^{-1/2}$ [19]. For avoiding the computational nodes in the vicinity of the body to slip away from the boundary layer, the mesh velocities adjacent to the body are expediently assigned to be equal to the velocity of the body.

A brief outline of the solution procedure is described as follows:

1. Determine the optimal mesh distribution and number of the elements and nodes.
2. Solve the values of the U, V and θ at the steady state and regard them as the initial values.
3. Determine the time increment $\Delta\tau$ and the mesh velocities of the computational meshes.
4. Update the coordinates of the nodes and examine the determinant of the Jacobian transformation matrix and ensure the one-to-one mapping to be satisfied during the Gaussian quadrature numerical integration. Execute the mesh reconstruction as the deformation of the meshes affects the accuracy of the results.
5. Use the numerical method mentioned above to solve Eq. (10) until the following criterion for convergence are satisfied:

$$\left|\frac{\phi^{m+1}-\phi^m}{\phi^{m+1}}\right|_{\tau+\Delta\tau}<10^{-3}, \quad \text{where } \phi=U, V, \tag{14}$$

and substitute the U and V into Eq. (12) to obtain θ.

6. Continue the next time step, calculate until the assigned time is reached.

4. Results and discussion

The working fluid is air with $Pr=0.71$. For matching the boundary conditions at the inlet and outlet of the channel mentioned earlier, at the time $\tau=0.0$ the dimensionless lengths of $H\,(=\frac{h}{l})$ and $D\,(=\frac{d}{l})$ are determined by the numerical tests and equal to 31 and 20, respectively. The dimensionless width $W\,(=\frac{w}{l})$ of the channel is 10.

The local Nusselt number Nu_X and the average local Nusselt number $\overline{Nu_X}$ on the top surface (FH) or the bottom surface (EG) of the body at the time τ are defined as follows.

$$Nu_X=-\frac{\partial\theta}{\partial Y}, \tag{15}$$

$$\overline{Nu_X} = \frac{1}{L}\int_0^L Nu_X \, dX. \tag{16}$$

The local Nusselt number Nu_Y and the average local Nusselt number $\overline{Nu_Y}$ on the lateral surface (EF or GH) of the body at the time τ are defined as follows.

$$Nu_Y = -\frac{\partial \theta}{\partial X}, \tag{17}$$

$$\overline{Nu_Y} = \frac{1}{L}\int_0^L Nu_Y \, dY. \tag{18}$$

The average global Nusselt number Nu on the surfaces of the body at the time τ is defined as

$$Nu = \frac{1}{4L}\left(\int_{FH} Nu_X \, dX + \int_{EG} Nu_X \, dX + \int_{EF+GH} Nu_Y \, dY\right). \tag{19}$$

The mean global Nusselt number $\overline{Nu}$ for the duration of the transient development on the surface of the body is defined as

$$\overline{Nu} = \frac{1}{\tau}\int_0^\tau Nu \, d\tau. \tag{20}$$

In order to obtain the optimal mesh, the nonuniform distribution elements of 1872, 2672 and 3904 (corresponding to 7720, 10,952 and 15,944 nodes, respectively) are used for grid tests at steady state and $Re = 500$ situation. The distribution of U, V and θ along the line MN as shown in Fig. 1 are indicated in Fig. 2. According to the results of the grid tests, the computational mesh with 3904 elements is adopted. As for the selection of time step $\Delta\tau$, four different time steps of 0.01, 0.005, 0.0025, 0.001 with $Re = 500$ and the moving velocity of the body $V_b = 2.0$ are adopted, and the results are shown in Fig. 3. The variation of the average local Nusselt numbers with time on each surface of the body are consistent for the above differ-

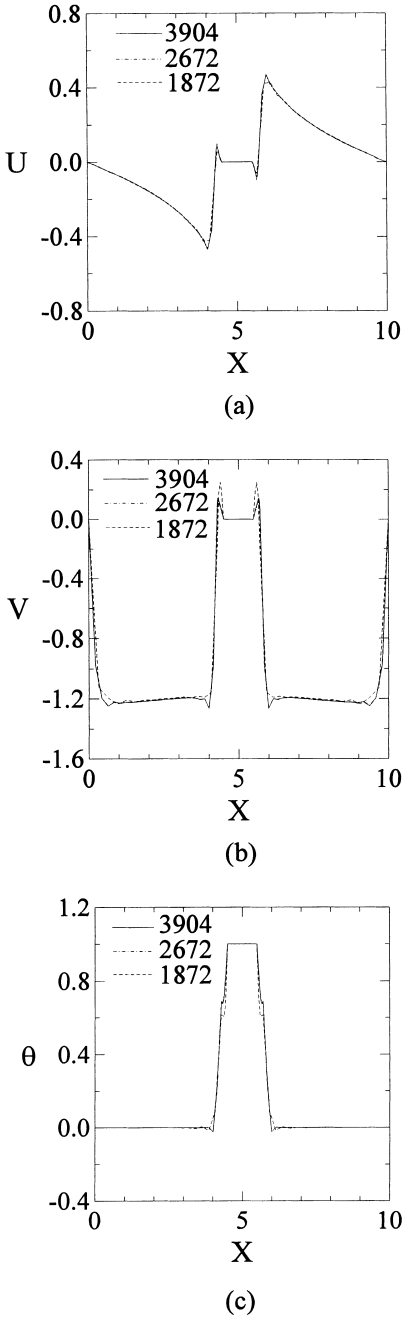

Fig. 2. Comparison of the variation of the U, V and θ distributions along the line MN at steady state and $Re = 500$ for various meshes.

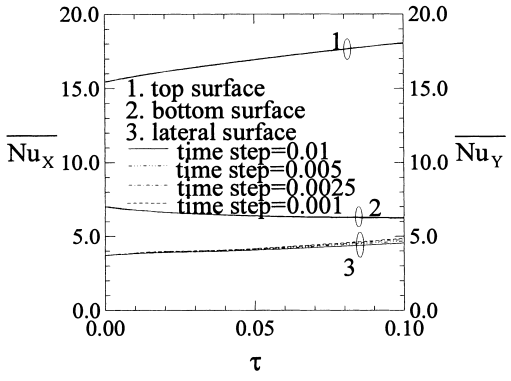

Fig. 3. Comparison of the variation of the average local Nusselt numbers on each surface of the body with different time steps $\Delta\tau$ for $Re = 500$ and $V_b = 2.0$.

ent time steps, and the time step of 0.005 is chosen. In addition, the dimensionless time duration of the transient development is 1.0.

To limit the contents of the study, the flow and heat transfer mechanisms are mainly focused on the $V_b = 0.5$ and 2.0, and $Re = 500$ situations. To illustrate the flow and thermal fields more clearly, only the phenomena in the vicinity of the body are presented.

Shown in Fig. 4 is the transient development of the velocity vectors around the body for the $V_b = 0.5$ case. Recirculation zones in the vicinity of the bottom surface of the body and reverse flow zones near the lateral surface of the body are observed apparently at the steady state ($\tau = 0.0$). At the beginning of the transient state, the body moves upward and pushes the fluids near the top surface of the body, and this fluid flows upward and the direction of this motion is opposite to that of the inlet fluid, where the flow direction is downward. As a result, the upward and downward flows become opposing flows. Since the magnitude of the inlet fluid is larger, the upward fluid motion mentioned above is deflected and becomes a downward flow in a short distance away from the body.

As for the fluid near the bottom surface of the body, the flow impinges the bottom surface and turns the flow direction to the lateral sides at the steady state as shown in Fig. 4(a). The fluid near the bottom surface of the body is continuously replenished from both the bottom and lateral sides as the body moves upward. The velocities of the fluid close to the bottom surface are usually smaller than the moving velocity of the body, and new recirculation zones are formed around the corners of the bottom surface. Consequently, the situation where the fluid impinges on the bottom surface at the steady state no longer occurs, which is disadvantageous to the heat transfer.

As for the behavior of the fluid near the lateral surface of the body, a slight reverse flow is observed along the lateral surface at the steady state. As the body begins to move upward, a new recirculation zone is formed near the upper corner of the lateral surface due to the interaction of the body moving upward and the fluid flowing downward, and a reattachment region exists on the lateral surface. Further, the recirculation zone gradually grows larger and stronger and moves from the upper to the lower corners of the lateral surface. In the meantime, the fluid adhering to the lateral surface flows with the lateral surface; the flow direction of the fluid near the lateral is upward. The fluid near the low corner of the lateral surface replenishes the vacant space near the bottom surface induced by the movement of the body, and the flow directions of this fluid becomes downward and differ from those at the steady state mentioned above.

The transient development of the isothermal lines around the body for the $V_b = 0.5$ case is shown in Fig. 5. The variation of the thermal fields usually corresponds to the variation of the velocity fields. The distribution of the isothermal lines is dense near the top surface of the body due to the collision of the upward and downward flows mentioned above. This flow turns near the corners of the top surface and the distribution

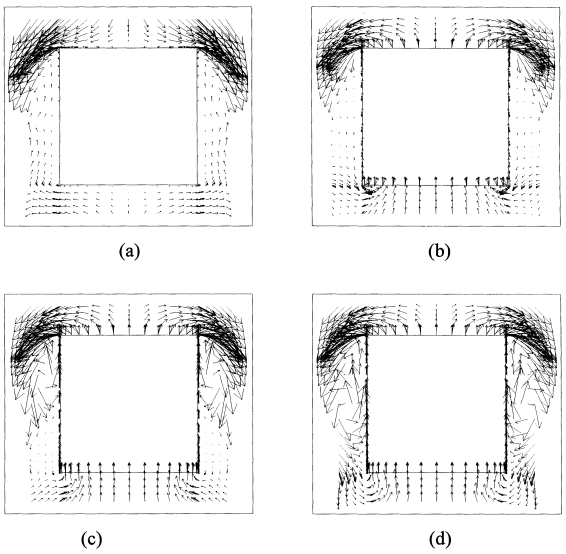

Fig. 4. The transient development of the velocity vectors around the body for $Re = 500$ and $V_b = 0.5$ case (a) $\tau = 0.0$, (b) $\tau = 0.05$, (c) $\tau = 0.5$, (d) $\tau = 1.0$.

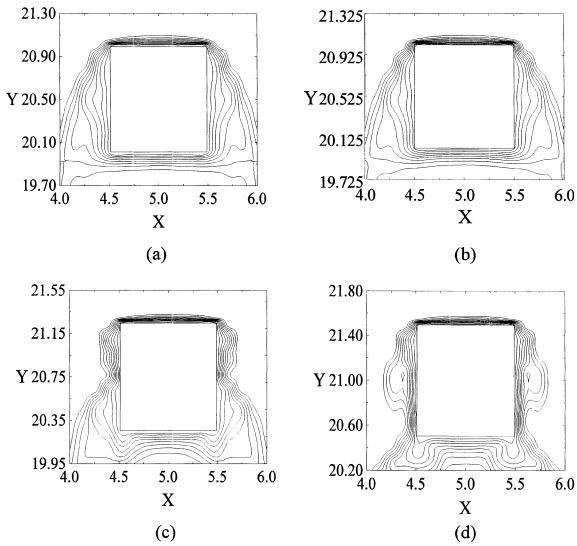

Fig. 5. The transient development of the isothermal lines around the body for $Re = 500$ and $V_b = 0.5$ case (a) $\tau = 0.0$, (b) $\tau = 0.05$, (c) $\tau = 0.5$, (d) $\tau = 1.0$.

of the isothermal lines becomes denser near the corner regions. During the duration of the motion, the distribution of the isothermal lines near the top surface is still denser than those near the other surfaces. Most of the fluid behind the body does not catch up to the bottom surface due to the movement of the body and the density of the isothermal lines becomes sparse. The recirculation zones that exist near the corners of the bottom surface cause the isothermal lines to extend outside. The fluid in the neighborhood of the lateral surface flow with the movement of the lateral surface, which is similar to the fluid flowing through a plate. Therefore, the distribution of the isothermal lines close to the lateral surface is denser than those near the bottom surface.

The results of the transient development of the local Nusselt number Nu_X and Nu_Y on the surfaces of the body for the $V_b = 0.5$ case are indicated in Figs. 6 and 7, respectively. The solid and dashed lines in Fig. 6 indicate the results of the top and bottom surfaces, respectively. The opposing flow mentioned earlier is similar to an impinging flow that enhances the heat transfer rate on the top surface doubtlessly, the local Nusselt numbers distributions on the top surface then increase with the increment of time. On the other side, the flow no longer impinges on the bottom surface and the recirculation zones appear near the corners of the bottom surface, which causes the distribution of the local Nusselt numbers on the bottom surface at the steady state to be larger than those of the transient development.

In Fig. 7, the results of the local Nusselt number Nu_Y on the lateral surface are shown. At the steady state (Fig. 7(a)), the situation is similar to the fluid flowing through a plate with finite length, and the larger local Nusselt numbers are distributed on the upper and lower edges of the lateral surface and the smaller local Nusselt numbers are distributed on the central region. As the body starts to move, the upstream fluid has higher downward velocities and flow over the upper edge of the lateral surface as shown in Fig. 4. This motion decelerates the upward velocities of the fluid, which are close to the lateral surface. Consequently, in the early stages the enhancement of the local Nusselt numbers on the lateral surface induced by the upward movement of the body is not so apparent. The enhancement regions near the lateral surface change from the upper to the lower regions of the lateral surface due to the variation of the recirculation zones and reattachment regions and gradually become apparent.

The transient development of the average local Nusselt number $\overline{Nu_X}$ and $\overline{Nu_Y}$ on the surfaces of the body for the $V_b = 0.5$ case are indicated in Fig. 8. Based upon the reasons mentioned earlier, the average local Nusselt numbers distributed on the top and lateral surfaces under the transient development are enhanced, and the maximum magnitudes of the enhancement are about 25% and 175%, respectively. Conversely, the average local Nusselt numbers distributed on the bot-

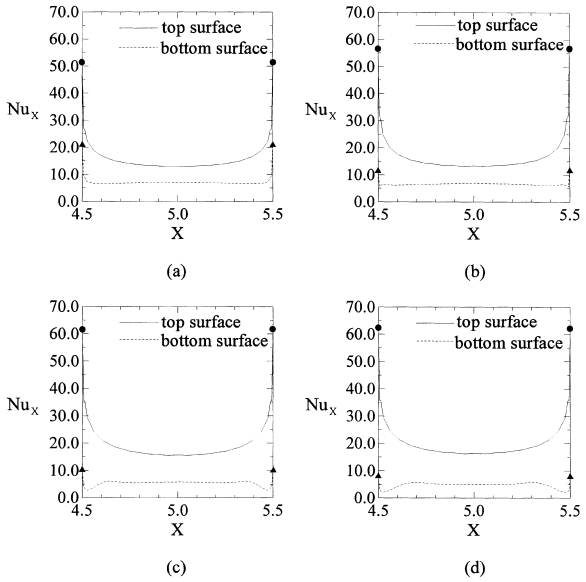

Fig. 6. The transient development of the local Nusselt numbers Nu_X on the top and bottom surfaces for $Re = 500$ and $V_b = 0.5$ case (a) $\tau = 0.0$, (b) $\tau = 0.05$, (c) $\tau = 0.5$, (d) $\tau = 1.0$.

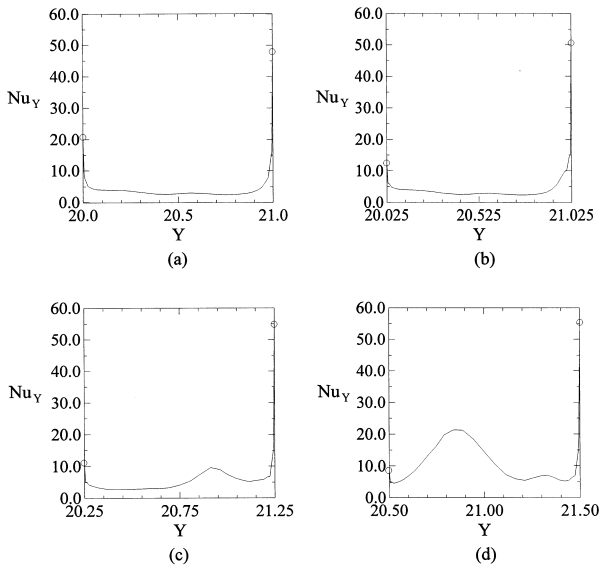

Fig. 7. The transient development of the local Nusselt numbers Nu_Y on the lateral surface of the body for $Re = 500$ and $V_b = 0.5$ case (a) $\tau = 0.0$, (b) $\tau = 0.05$, (c) $\tau = 0.5$, (d) $\tau = 1.0$.

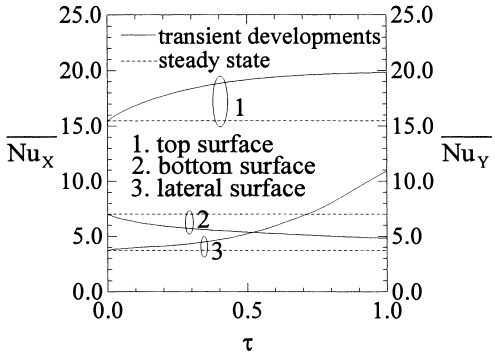

Fig. 8. The transient development of the average local Nusselt numbers on the surfaces of the body for $Re = 500$ and $V_b = 0.5$ case.

tom surface under the transient developments are decreased, and the maximum magnitude of the decrement is about 33%.

The transient development of the average global Nusselt number Nu of the body for the $V_b = 0.5$ case is shown in Fig. 9. The average global Nusselt numbers of the body under the transient development are larger than that at the steady state, and the maximum magnitude of the enhancement is about 50%. The mean increments of the average global Nusselt numbers are about 20%.

Shown in Fig. 10 is the transient development of the velocity vectors around the body for the $V_b = 2.0$ case. Since the moving velocity of the body V_b $(= 2.0)$ is greater than that of the above case $(V_b = 0.5)$, the variation of the flow fields near the body is more drastic in this case. The flow field near the top surface of the body in this case is similar to that of the $V_b = 0.5$ case. As for the fluid near the bottom surface of the body, recirculation zones are formed around the corners of the bottom surface at first, and the recirculation zones grow larger. After that, most of the fluid that fills the vacant space induced by the movement of the body are provided from the region behind the body, which is like the situation of the flow impinging on the bottom surface. As a result, the recirculation zones vanish, and the phenomena are different from those of the above case as shown in Fig. 4; this is an advantage to the heat transfer mechanism. Concerning the fluid near the lateral surface of the body, the behavior of the fluid is similar to but more drastic than that of the above case.

The transient development of the average local Nusselt number $\overline{Nu_X}$ or $\overline{Nu_Y}$ for the $V_b = 2.0$ case are indicated in Fig. 11. According to the reasons mentioned earlier, the variation of the average local Nusselt numbers on the top surface is similar to that of the case of $V_b = 0.5$. On the bottom surface, the average local Nusselt numbers distributed on the bottom surface decrease with time in the initial duration since the fluid cannot catch up to the central region of the bottom surface and the recirculation zones are formed around the corners of the bottom surface. As the time increases, the recirculation zones around the corners of the bottom surface vanish, and the average local Nusselt numbers distributed on the bottom surface then increase a little. As for the lateral surface, the average

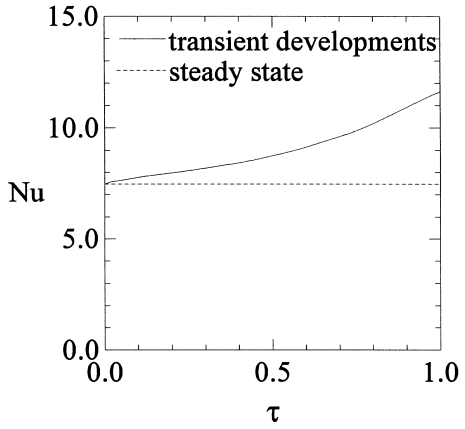

Fig. 9. The transient development of the average global Nusselt number of the body for $Re = 500$ and $V_b = 0.5$ case.

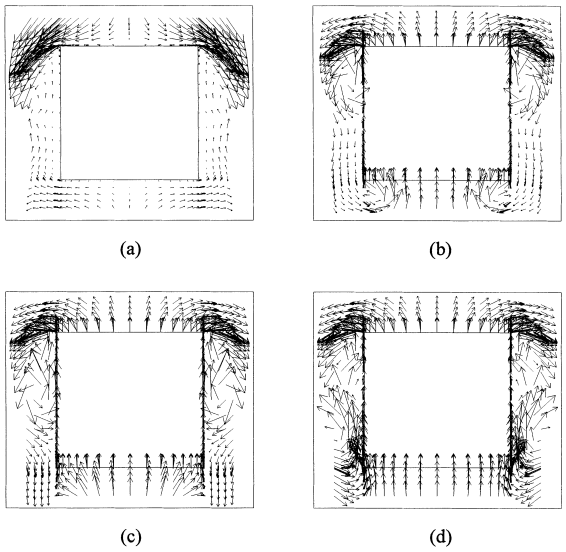

Fig. 10. The transient development of the velocity vectors around the body for $Re = 500$ and $V_b = 2.0$ case (a) $\tau = 0.0$, (b) $\tau = 0.25$, (c) $\tau = 0.5$, (d) $\tau = 1.0$.

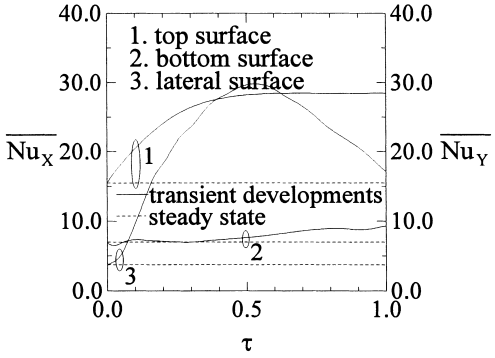

Fig. 11. The transient development of the average local Nusselt numbers on the surfaces of the body for $Re = 500$ and $V_b = 2.0$ case.

local Nusselt numbers are increased at the beginning of the motion. For times τ is larger than 0.5, the fluid near the lateral surface flow with the lateral surface and the reattachment region is destroyed, which causes the average local Nusselt numbers to decrease.

The variation of the average global Nusselt number Nu of the body for the $V_b = 2.0$ case is shown in Fig. 12. The increment of the average local Nusselt numbers on the top and lateral surfaces are large which cause the average global Nusselt numbers during the transient development to be larger than those at the steady state. The mean increment of the average global Nusselt number is about 140%, which is larger than that of the $V_b = 0.5$ case.

Several different Reynolds numbers and the moving velocities of the body are taken into consideration in determining the relationship among the three variables of the mean global Nusselt number $\overline{Nu}$, Reynolds

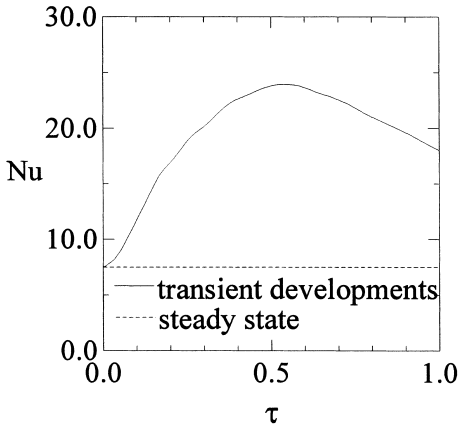

Fig. 12. The transient development of the average global Nusselt number of the body for $Re = 500$ and $V_b = 2.0$ case.

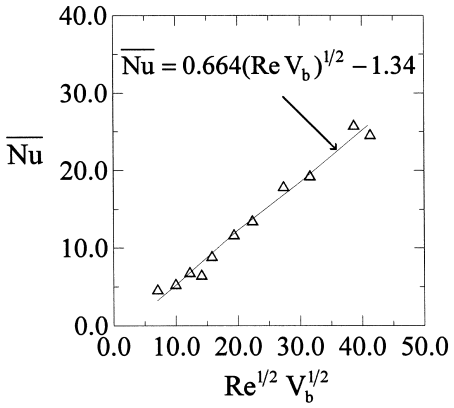

Fig. 13. The relationship between the mean global Nusselt number $\overline{Nu}$ and $Re^{1/2}\,V_b^{1/2}$.

number Re and the moving velocity of the body V_b for the duration of the transient development. The results are shown in Fig. 13. The relationship between the mean global Nusselt number $\overline{Nu}$ and $Re^{1/2}\,V_b^{1/2}$ can be correlated by an equation of

$$\overline{Nu} = 0.664(Re\,V_b)^{1/2} - 1.34. \tag{21}$$

5. Conclusions

The heat transfer rate of a body moving in opposition to a flowing fluid is studied numerically. Some conclusions are summarized as follows:

1. The fluid near the bottom and lateral surfaces of the body simultaneously replenish the vacant space induced by the movement of the body, and new recirculation zones are formed near the corners of the bottom and lateral surfaces of the body. These phenomena are apparently different from those of the body fixed in the flowing fluids.
2. The enhancement of the heat transfer rate of a body moving in opposition to a flowing fluid is remarkable.
3. The relationship between the mean global Nusselt number $\overline{Nu}$ of the body and $Re^{1/2}\,V_b^{1/2}$ is linear.

Acknowledgements

The support of this work by the National Science Council of Taiwan, Republic of China, under contract NSC87-2212-E-009-035 is gratefully acknowledged.

References

[1] W.F. Noh, A time-dependent two-space-dimensional coupled Eulerian–Lagrangian code, in: B. Alder, S. Fernbach, M Rotenberg (Eds.), Methods in Computational Physics 3, Academic Press, New York, 1964, p. 117.

[2] C.W. Hirt, A.A. Amsden, H.K. Cooks, An arbitrary Lagrangian–Eulerian computing method for all flow speeds, Journal of Computational Physics 14 (1974) 227–253.

[3] T.J.R. Hughes, W.K. Liu, T.K. Zimmermann, Lagrangian–Eulerian finite element formulation for incompressible viscous flows, Computer Methods in Applied Mechanics and Engineering 29 (1981) 329–349.

[4] A. Huerta, W.K. Liu, Viscous flow with large free surface motion, Computer Methods in Applied Mechanics and Engineering 69 (1988) 277–324.

[5] B. Ramaswamy, Numerical simulation of unsteady viscous free surface flow, Journal of Computational Physics 90 (1990) 396–430.

[6] T. Belytschko, D.P. Flanagan, J.M. Kennedy, Finite element methods with user-controlled meshes for fluid–structure interaction, Computer Methods in Applied Mechanics and Engineering 33 (1982) 669–688.

[7] J. Donea, S. Giuliani, J.P. Halleux, An arbitrary Lagrangian–Eulerian finite element method for transient dynamic fluid structure interactions, Computer Methods in Applied Mechanics and Engineering 33 (1982) 689–723.

[8] A. Huerta, W.K. Liu, Viscous flow structure interaction, Journal of Pressure Vessel Technology 110 (1988) 15–21.

[9] T. Nomura, T.J.R. Hughes, An arbitrary Lagrangian–Eulerian finite element method for interaction of fluid and a rigid body, Computer Methods in Applied Mechanics and Engineering 95 (1992) 115–138.

[10] T. Nomura, Finite element analysis of vortex-induced vibrations of bluff cylinders, Journal of Wind Engineering and Industrial Aerodynamics 46 (1993) 587–594.

[11] A. Masud, T.J.R. Hughes, A space-time Galerkin/least-squares finite element formulation of the Navier–Stokes equation for moving domain problems, Computer Methods in Applied Mechanics and Engineering 146 (1997) 91–126.

[12] W.K. Liu, H. Chang, J.S. Chen, T. Belytschko, Arbitrary Lagrangian–Eulerian Petrov–Galerkin finite elements for nonlinear continua, Computer Methods in Applied Mechanics and Engineering 68 (1988) 259–310.

[13] W.K. Liu, J.S. Chen, T. Belytschko, Y.F. Zhang, Adaptive ALE finite elements with particular reference to external work rate on frictional interface, Computer Methods in Applied Mechanics and Engineering 93 (1991) 189–216.

[14] S. Chippada, T.C. Jue, B. Ramaswamy, Finite element simulation of combined buoyancy and thermocapillary driven convection in open cavities, International Journal for Numerical Methods in Engineering 38 (1995) 335–351.

[15] W.J. Mascarenhas, H.U. Akay, M.J. Pikal, A computational model for finite element analysis of the freeze–drying process, Computer Methods in Applied Mechanics and Engineering 148 (1997) 105–124.

[16] J.N. Reddy, An Introduction to the Finite Element Method, 2nd ed., McGraw-Hill, New York, 1993, pp. 488–494.

[17] J.N. Reddy, D.K. Gartling, The Finite Element Method in Heat Transfer and Fluid Dynamics, CRC Press, Ann Arbor, 1994, pp. 47–51.

[18] W.S. Fu, T.M. Kau, W.J. Shieh, Transient laminar natural convection in an enclosure from steady state to stationary state, Numerical Heat Transfer: Part A 18 (1990) 189–212.

[19] H. Schlichting, Boundary Layer Theory, 7th ed., McGraw-Hill, New York, 1979 (Chapter 5).